Applied Energy 113 (2014) 106–115

Contents lists available at SciVerse ScienceDirect

Applied Energy

journal homepage: www.elsevier.com/locate/apenergy

State of charge estimation of lithium-ion batteries using the open-circuit voltage at various ambient temperatures

Yinjiao Xing [a,*], Wei He [b], Michael Pecht [b], Kwok Leung Tsui [a]

[a] Department of Systems Engineering and Engineering Management, City University of Hong Kong, 83 Tat Chee Avenue, Kowloon, Hong Kong
[b] Center for Advanced Life Cycle Engineering (CALCE), University of Maryland, College Park, MD 20740, USA

HIGHLIGHTS

- An offline OCV–SOC–temperature table was established to infer battery SOC.
- A temperature-based model was developed to estimate SOC at different temperatures.
- The algorithm for SOC estimation was verified by dynamic current load.
- The robustness of the approach was validated by different initial SOC values.

GRAPHICAL ABSTRACT

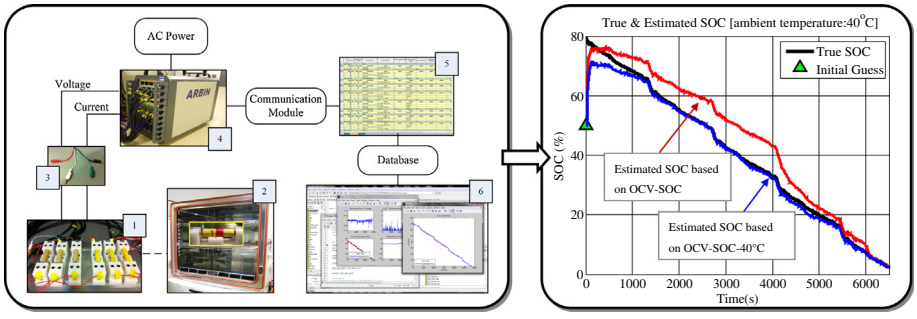

ARTICLE INFO

Article history:
Received 2 April 2013
Received in revised form 28 June 2013
Accepted 3 July 2013
Available online 7 August 2013

Keywords:
Electric vehicles
Lithium-ion batteries
SOC estimation
Open-circuit voltage
Temperature-based model
Unscented Kalman filtering

ABSTRACT

Ambient temperature is a significant factor that influences the accuracy of battery SOC estimation, which is critical for remaining driving range prediction of electric vehicles (EVs) and optimal charge/discharge control of batteries. A widely used method to estimate SOC is based on an online inference of open-circuit voltage (OCV). However, the fact that the OCV–SOC is dependent on ambient temperature can result in errors in battery SOC estimation. To address this problem, this paper presents an SOC estimation approach based on a temperature-based model incorporated with an OCV–SOC–temperature table. The unscented Kalman filtering (UKF) was applied to tune the model parameters at each sampling step to cope with various uncertainties arising from the operation environment, cell-to-cell variation, and modeling inaccuracy. Two dynamic tests, the dynamic stress test (DST) and the federal urban driving schedule (FUDS), were used to test batteries at different temperatures. Then, DST was used to identify the model parameters while FUDS was used to validate the performance of the SOC estimation. The estimation was made covering the major working range from 25% to 85% SOC. The results indicated that our method can provide accurate SOC estimation with smaller root mean squared errors than the method that does not take into account ambient temperature. Thus, our approach is effective and accurate when battery operates at different ambient temperatures. Since the developed method takes into account the temperature factor as well as the complexity of the model, it could be effectively applied in battery management systems for EVs.

1. Introduction

Electric vehicles (EVs) are bringing new life to the automobile industry as an alternative way to reduce consumption of fossil fuels. As one of the critical components in EVs, battery performance determines the safety, reliability, and operating efficiency of the vehicle system. Accurate and instantaneous information on the state of the battery, such as state of charge (SOC) and state of health (SOH), should be provided to the drivers by a battery management system (BMS) to guarantee safe and reliable battery operation. [1–4]. The SOC quantifies the usable energy at the present

* Corresponding author. Tel.: +852 3442 5934; fax: +852 3442 0272.
E-mail addresses: yxing3@student.cityu.edu.hk (Y. Xing), weihe@calce.umd.edu (W. He), pecht@calce.umd.edu (M. Pecht), kltsui@cityu.edu.hk (K.L. Tsui).

0306-2619/$ - see front matter © 2013 Elsevier Ltd. All rights reserved.
http://dx.doi.org/10.1016/j.apenergy.2013.07.008

cycle, while the SOH denotes the remaining performance of the battery over its whole life cycle [5]. Battery SOC is a direct and immediate look at the remaining charge of the battery, which reflects residual range of an EV. This has gained more attention due to drivers' range anxiety i.e. running out of power on the road. Additionally, an accurate SOC is an indicator of how to improve a battery's operational reliability, extend its lifespan, and optimize the power management of the vehicle [1,2,6]. However, SOC cannot be measured directly but must be estimated according to measurable parameters such as current and voltage. Moreover, ambient temperature is a critical factor that affects the accuracy of SOC estimation [7–12].

There are three main types of methods for SOC estimation: coulomb counting, machine learning methods, and their combination using a model-based estimation approach. These three types of methods are described below.

Coulomb counting is a straightforward method for estimating SOC that accumulates the net charge at the last time period in units of ampere-hours (Ah). Its performance is highly reliant on the precision of current sensors and the accurate estimation of the initial SOC [3,13]. However, coulomb counting is an open-loop estimator that does not eliminate the accumulation of measurement errors and uncertain disturbances. In addition, it is not able to determine the initial SOC, and address the variation of the initial SOC caused by self-discharging. Without the knowledge of the initial SOC, this method will cause accumulating errors on SOC estimation. Taking into account these factors, regular recalibration is recommended and widely used by methods such as fully discharging the battery, or referring to other measurements such as open-circuit voltage (OCV), as suggested in [3,6,7,14].

Machine learning approaches, including artificial neural networks, fuzzy logic–based models, and support vector machines, have been used to estimate SOC online. Li et al. [15] designed a 12-input-2-level merged fuzzy neural network (FNN) that was fused with a reduced-form generic algorithm (RGA) to estimate SOC. Bo et al. [16] developed parallel chaos immune evolutionary programming (PICEP) to train a neural network model in which five input variables were selected. This approach was used to estimate the SOC of nickel–metal hydride (Ni/MH) batteries. The performance of the kind of black-box models is reliant on the reliability of the training data, i.e. whether it is sufficient to cover the entire loading conditions. Once the battery operated at the unknown loading conditions, the robustness of these models was subject to challenge. Wang [17] employed a support vector machine to model the dynamic behavior of a Ni/MH battery under dynamic current loading. However, model training is time consuming and requires a large amount of data. Also, the estimation based on this model causes a large prediction error due to the uncertainty of the new data set.

A model-based filtering estimation approach is being widely applied due to its close-loop nature and concerning various uncertainties. Both electrochemical models and equivalent circuit models aim to capture the dynamic behavior of the battery. The former are usually presented in the form of partial differential equations with many unknown parameters. They are accurate but not desirable in practice because of a high requirement for memory and computation. To guarantee the accuracy of the model and the feasibility, equivalent circuit models have been implemented in BMSs such as the enhanced self-correcting (ESC) model and the hysteresis model, as found in [10,18,19], and one or two-order resistance–capacitance (RC) network models [1,2,10,11,20]. OCV is a vital element in the above-mentioned battery equivalent models and is a function of SOC in nature. The premise of utilizing OCV–SOC is that the battery needs to rest a long time and terminal voltage approaches the OCV. However, in real life, a long resting time may not be possible. To make up for the flaws of OCV methods, nonlinear filtering techniques based on state-space models have been developed to enhance SOC estimation through combining coulomb counting and OCV [7]. Plett applied extended Kalman filters (EKF) into BMS to implement SOC estimation of a lithium polymer battery (LiPB) using different battery models in [10,21,22]. Plett later proposed the use of two sigma-point Kalman filtering (SPKF) estimators, including the unscented Kalman filter (UKF) and central difference Kalman filter (CDKF), in [18,23]. Subsequently, adaptive EKF [7,20], dual EKF [11], and adaptive UKF [3] were developed to improve the accuracy of the SOC estimation based on their own sample sets and some common equivalent circuit models. Charkhgard and Farrokhi [13] also proposed the combination of NN and EKF to estimate SOC. NN was employed to train a lithium-ion battery model using some charging data from the battery. The effectiveness of this method was not verified under the dynamic discharging data, which would lead to a larger uncertainty on estimating SOC.

However, several existing issues are seldom addressed in the literature. Firstly, the temperature dependence of the OCV–SOC lookup table is seldom discussed with regard to battery SOC estimation. Instead, a single OCV–SOC table constructed at a certain temperature (e.g., room temperature) is widely employed. It will cause a large error in inferring SOC when the battery is operating at other ambient temperatures (not room temperature) [1,8,10,11]. Secondly, lithium-ion batteries have a relatively flat OCV curve over the SOC, especially for lithium iron phosphate ($LiFePO_4$) batteries, which are widely used in the electric vehicle market [24]. That means a small error on the inferred OCV will produce a larger deviation in SOC. Thirdly, different models were adopted by individuals based on their own experimental data. Although a sophisticated model with more parameters might be able to provide a smaller modeling error, it would run the risk of adding more uncertainties, such as over-fitting problems and the introduction of unnecessary noises, especially concerning temperature. Therefore, it makes more sense to investigate a generic but accurate temperature-based model with fewer parameters for real-time applications. Kim et al. [25] considered temperature as an input variable into a first-order RC circuit model. However, the effect of temperature on the OCV–SOC was ignored due to a slight difference between OCV curves from 30% SOC to 80% at different temperatures. Moreover, their samples have an obvious linear slope of OCV–SOC that is prone to infer SOC accurately. Nevertheless, for a relatively flat OCV curve dependent on ambient temperature, it is significant not only to develop an accurate and generic model considering ambient temperature, but also to enhance the capability of online estimation due to the uncertainty, including unit-to-unit variation, measurement noise, operational uncertainties, and model inaccuracy [26].

In this paper, a temperature-based internal resistance (R_{int}) battery model combined with a nonlinear filtering method was put forward to improve the SOC estimation of lithium-ion batteries under dynamic loading conditions at different ambient temperatures. The research proceeds as follows. Three tests at different temperatures are introduced in Section 2. The dynamic stress test (DST) and federal urban driving schedule (FUDS) are two kinds of dynamic loading conditions tested at different temperatures to identify the model parameters and verify the estimated performance, respectively. The purpose of the OCV–SOC–temperature (OCV–SOC–T) test is to extend the OCV–SOC behavior to temperature field. Due to various uncertainties of the system, UKF-based SOC estimator is proposed due to its superiority of reaching to the 3rd order of any nonlinearity over the EKF. The implemented procedure for our battery study is followed by Section 3. The experimental results are presented in Section 4 to compare our developed method based on OCV–SOC–T with the original

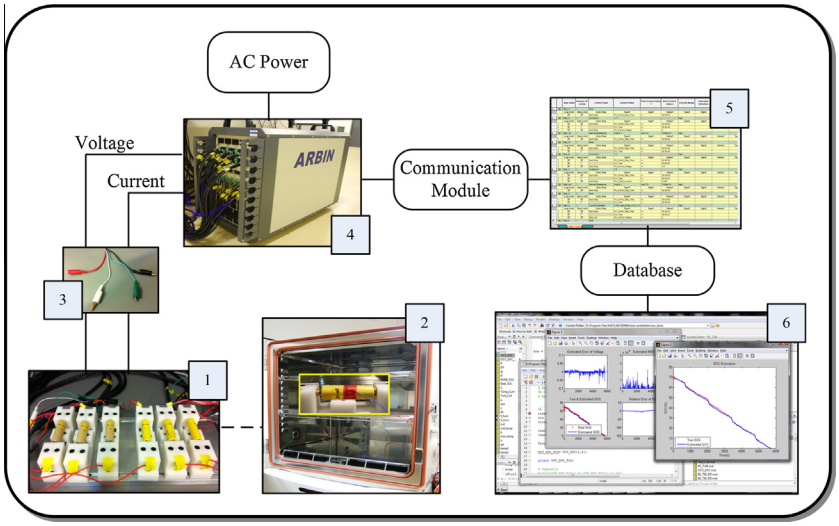

Fig. 1. Schematic of the battery test bench.

Table 1
The key specifications of the test samples.

Type	Nominal voltage	Nominal capacity	Upper/lower cut-off voltage	Maximum continuous discharge current
$LiFePO_4$	3.3 V	1.1Ah	3.6 V/2.0 V	30A

estimation using a single OCV–SOC table. The robustness is validated and compared under the different initial true values and different initial guesses of SOC.

2. Experiments

The experiment setup is shown in Fig. 1. It consisted of (1) lithium-ion cells (LiFePO4) of the 18650 cylindrical type (the key specifications are shown in Table 1); (2) Vötsch temperature test chamber (The cells were placed in cell holders in the chamber); (3) a current and voltage sampling cable for loading and sampling; (4) a battery test system (Arbin BT2000 tester); (5) a PC with Arbins' Mits Pro Software (v4.27) for battery charging/discharging control; (6) Matlab R2009b for data analysis. During battery operation, the sampling time of current, voltage was 1 s. Three separate test schedules were conducted on the battery test bench for model identification, OCV–SOC–*T* table construction, and method validation, respectively.

2.1. Model identification test

For model identification, the dynamic stress test (DST) was run from 0 °C to 50 °C at an interval of 10 °C. DST is employed to investigate the dynamic electric behavior of the battery. It is designed by US Advanced Battery Consortium (USABC) to simulate a variable-power discharge regime that represents the expected demands of an EV battery [27]. A completed DST cycle is 360 s long and can be scaled down to any desired maximum demand regarding the specifications of the test samples. Therefore, in our study, DST was run continuously from 100% SOC at 3.6 V to empty at 2 V over several cycles in a discharge process. The positive current responds to discharging while the negative denotes charging. The measured current and voltage profile at 20 °C is shown in Fig. 2.

2.2. The OCV–SOC–T test

OCV is a function of SOC for the cells. If the cell is able to rest for a long period until the terminal voltage approached the true OCV, OCV can be used to infer SOC accurately. However, this method is not practical for dynamic SOC estimation. To address this issue, the SOC can be estimated by combining the online identification of the OCV with the predetermined offline OCV–SOC lookup table. Taking into account the temperature dependence of the OCV–SOC table, the OCV–SOC test was conducted from 0 °C to 50 °C at an interval of 10 °C. The test procedure at each temperature is the same as follows. Firstly, the cell was fully charged using a constant current of 1C-rate (1C-rate means that a full discharge of the battery takes approximately 1 h) until the voltage reached to the cut-off voltage of 3.6 V and the current was 0.01 C. Secondly, the cell was fully discharged at a constant rate of C/20 until the voltage reached 2.0 V, which corresponds to 0% SOC. Finally, the cell was fully charged at a constant rate of C/20 to 3.6 V, which corresponds to 100% SOC. The terminal voltage of the cell is considered as a close approximation to the real equilibrium potential [6,10]. As shown

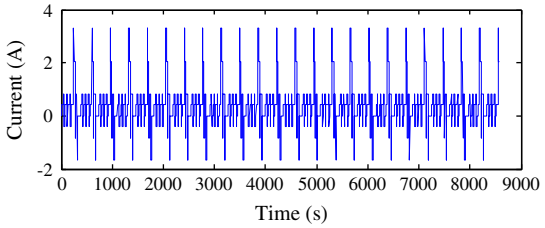

(a) Measured current

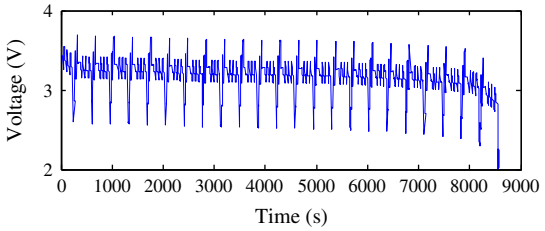

(b) Measured voltage

Fig. 2. DST profile at 20 °C.

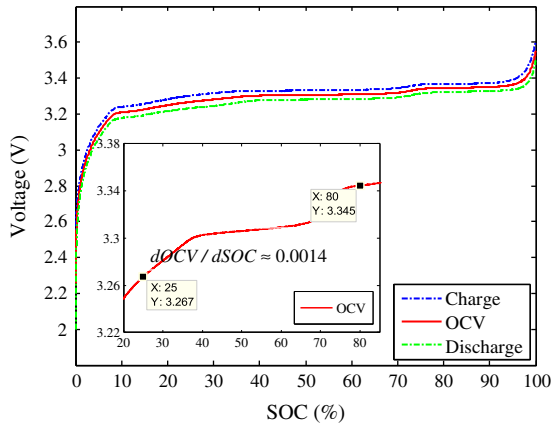

Fig. 3. OCV curve at 20 °C.

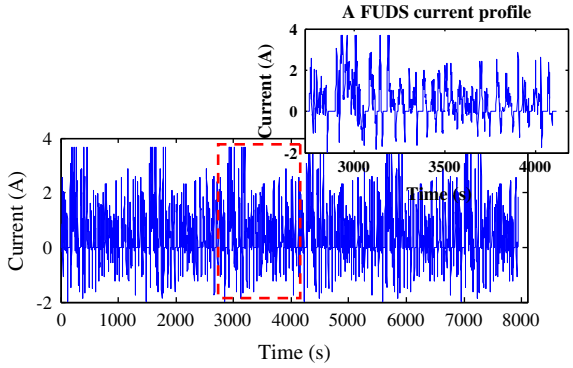

(a) Measured current

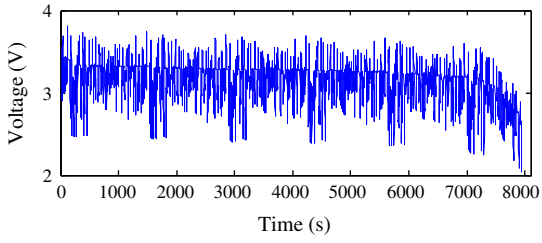

(b) Measured voltage

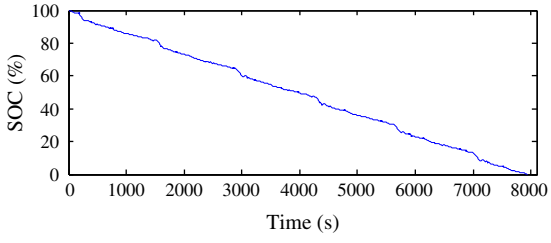

(c) Cumulative SOC

Fig. 4. FUDS profile at 20 °C.

in Fig. 3, the equilibrium potential during the charging process is higher than that during discharging process. It accounts for a hysteresis phenomenon of the OCV during the charging/discharging. In our paper, the OCV curve was defined as the average value of the charge and discharge equilibrium potentials. The effect of the hysteresis was ignored. In addition, referring to [28], when SOC is normalized relative to the specific cell capacity, the OCV–SOC curve can be referred to as being unique for the same type at the same testing condition. Fig. 3 shows the average OCV at 20 °C. A flat OCV slope between 25% and 80% SOC is emphasized in another small plot in Fig. 3. Its effect will be discussed in Section 3.1.

2.3. Method validation test

A validation test with a more sophisticated dynamic current profile, the federal urban driving schedule (FUDS), was conducted to verify the estimation algorithm based on the developed model. FUDS is a dynamic electric vehicle performance test based on a time–velocity profile from an automobile industry standard vehicle [27]. In the laboratory test, a dynamic current sequence was transferred from the time–velocity profile, programmed to charge or discharge the battery and applied to battery performance test [3,17,20,29]. Similar to the DST test, the current sequence is scaled to fit the specification of the test battery and the limitation of the testing system of Fig. 1. The current profile of FUDS causes variation of the SOC from fully charged at 3.6 V to empty at 2 V. The FUDS test was also run form 0 °C to 50 °C at an interval of 10 °C. The measured current, voltage profile, and the cumulative SOC at 20 °C are shown in Fig. 4. A completed FUDS current profile over 1372 s is emphasized in another graph in Fig. 4(a).

3. Battery modeling

For lithium-ion batteries, the internal resistance (R_{int}) model is generic and straightforward to characterize a battery's dynamics with one estimated parameter. Although a sophisticated model with more parameters would possibly show a well-fitting result, such as an equivalent circuit model with several amounts of parallel resistance–capacitance (RC) networks, it would also pose a risk of over-fitting and introducing more uncertainties for online estimation at the same time. Especially taking into account temperature factor, more complexity should be imposed on battery modeling. Therefore, we would prefer a simple model to a sophisticated model if the former had generalization ability and provided sufficiently good results. In this paper, model modification based on the original R_{int} model is proposed to balance the model complexity and the accuracy of battery SOC estimation. The schematic of the original R_{int} model is shown in Fig. 5.

$$U_{\text{term},k} = U_{\text{OCV}} - I_k \times R \tag{1}$$

$$U_{\text{OCV}} \propto f(\text{SOC}_k) \tag{2}$$

In Eqs. (1) and (2), $U_{\text{term},k}$ is the measured terminal voltage of the battery under a normal dynamic current load at time k, and I_k is the dynamic current at the same time. The positive current responds to discharging while the negative value means charging. R is the simplified total internal resistance of the battery. U_{OCV} is a function of SOC of the battery that should be tested following the procedure as presented in Section 2.2. The battery model Eq. (1) can be used to infer OCV directly according to the measured terminal voltage and the current of the battery. Then, the SOC can be estimated using $f^{-1}(U_{\text{OCV}})$, that is, the OCV–SOC lookup table.

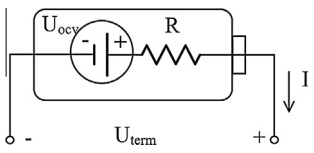

Fig. 5. Schematic of the internal resistance (R_{int}) model of the battery.

3.1. Model parameter identification

The DST was run on the $LiFePO_4$ batteries to identify the model parameter R in Eq. (1). Taking the current and voltage profile of DST at 20 °C as an example, the voltage and current are measured and recorded from fully charged to empty with a sampling period of 1 s based on our battery test bench. The accumulative charge (experimental SOC) is calculated synchronously from 100% SOC. Thus, the parameter R can be fitted using a sequence of the current, voltage, and the offline OCV–SOC by the least square algorithm. In terms of the fitted R value, the model performance can be evaluated based on the measured terminal voltage ($U_{\text{term},k}$) and the estimated voltage ($U_{\text{term},k}$). Fig. 6 shows the measured and the estimated voltage response on the DST profile at 20 °C based on the original model.

In statistics, the mean absolute error (MAE) and the root mean squared (RMS) error can be used together to evaluate the goodness-of-fit of the model. These two indicators are given by the following equations respectively.

$$\text{MAE} = \frac{1}{n}\sum_{k=1}^{n}|e_k| \tag{3}$$

$$\text{RMS error} = \sqrt{\frac{1}{n}\sum\nolimits_{k=1}^{n}(e_k)^2} \tag{4}$$

Here, e_k is the modeling error ($U_{\text{term},k} - U_{\text{term},k}$) at time k. The MAE measures how close forecasts are to the corresponding outcomes without considering the direction. The RMS error is more sensitive to large errors than the MAE. It is able to characterize the variation in errors. The statistics list of the model is shown in Table 2.

According to the small graph in Fig. 3, the OCV slope, namely, dOCV/dSOC is approximately equal to 0.0014 between 25% and 80% SOC. This means that the deviation on the OCV inference will cause an estimated deviation of SOC up to 21% when there is a MAE of 0.0288 V based on the current model. Additionally, a large mean error was plotted over time in Fig. 6. Thus, the residuals should be reduced to improve the model adequacy with smaller MAE and RMS error values.

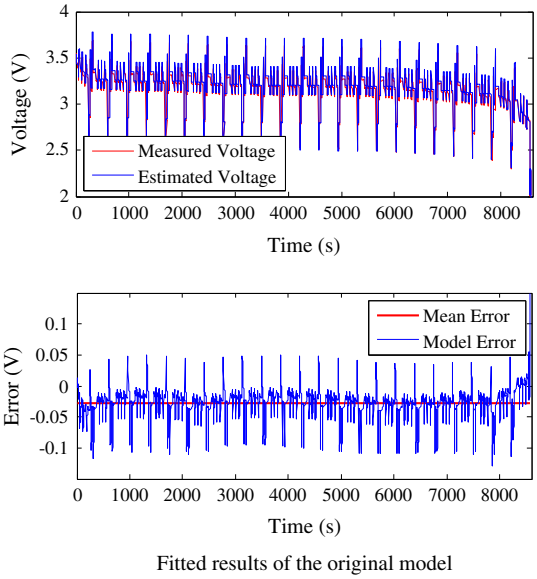

Fig. 6. The measured and the estimated voltage response on the DST profile based on the original model at 20 °C.

Table 2
Model parameter and statistics list of the fitted error of the model.

R (Ω)	Mean absolute error	RMS modeling error
0.2445	0.0288 V	0.0301

3.2. Model improvement and validation

3.2.1. The OCV–SOC–T table for model improvement

According to the test in Section 2.2, six OCV curves were obtained from 0 °C to 50 °C at an interval of 10 °C. Fig. 7(a) emphasizes the differences of OCV–SOC curves between 30% and 80% SOC at different temperatures. It can be seen that $SOC_{0°C}$ is much larger than other SOC values at higher temperatures when the OCV inference is the same, i.e., 3.3 V. It makes sense that the releasable capability of the charge is reduced at low temperatures. Fig. 7(b) shows the SOC values if the OCV inference was equal to the specific values from 3.28 V to 3.32 V at intervals of 0.01 V at three temperatures: 0 °C, 20 °C, 40 °C.

One issue of interest can be seen in Fig. 7(b). That is, the same OCV inference at different temperatures corresponds to different SOC values. For example, the SOC difference between 0 °C and 40 °C reaches approximately 22% at an OCV of 3.30 V. Therefore, we propose adding the OCV–SOC–T to the battery model to improve the model accuracy. The improved battery model is as follows:

$$U_{\text{term},k} = U_{\text{OCV}}(\text{SOC}_k, T) - I_k \times \text{R}(T) + \text{C}(T) \tag{5}$$

where U_{OCV} is a function of SOC and ambient temperature (T). $C(T)$ is a function of temperature that facilitates the reduction of the offset due to model inaccuracy and environmental conditions. Fig. 8 shows the measured and the estimated voltage response on the DST profile at 20 °C based on the proposed model. It can be found that the mean error of the new model is reduced with small variations as compared to the original model in Fig. 6.

Another issue of interest in Fig. 7(b) is that a small deviation of 0.01 V in OCV inference will lead to a large difference in SOC at the same temperature condition. It is the same issue as shown in Fig. 3. Therefore, if the SOC estimation were directly inferred from a battery model, it would have a high requirement on the model and measurement accuracy. To address this issue and improve the accuracy of the SOC estimation, the model-based unscented Kalman filtering approach was employed and introduced in Section 4.

3.2.2. The validation of the proposed model

Based on the developed model in Eq. (5), it is noted that the specific OCV–SOC look-up table should be selected in terms of the ambient temperature (here it is viewed as an average value). Least square fitting was also used to identify model parameters, R and C. The fitted model parameter list and the statistics list of the proposed model are shown in Table 3.

In comparison to the fitted results at 20 °C of Table 2, here the MAE is one order of magnitude smaller than that of the original model and the RMS modeling error is also reduced. In addition, the correlation coefficient (Corrcoef) was calculated for residual analysis. The Corrcoef(e_k, I_k) values close to zero indicate that the residuals and the input variable hardly have linear relationship. Thus, the corrected model can be better fitted on the dynamic current load. One finding of interest is C values that can be fitted over the ambient temperature (T) using a regression curve, as Fig. 9 shows. Referring to the paper [30], the exponential function can be selected to fit C values over T because the internal elements of the battery, i.e., battery resistance follow the Arrhenius equation, which has exponential dependency on the temperature. In our study, five C values at 0 °C, 10 °C, 20 °C, 25 °C, 30 °C, 40 °C were

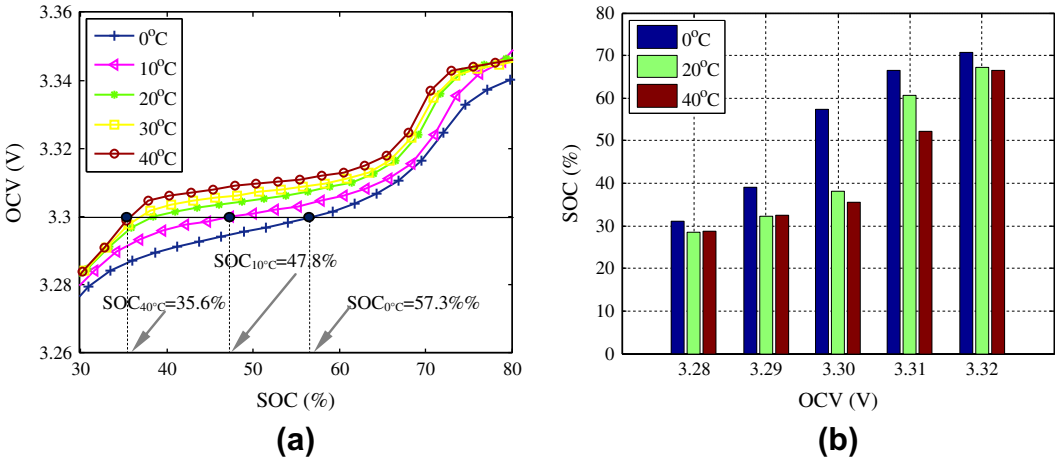

Fig. 7. (a) OCV–SOC curves between 30% and 80% SOC at different temperatures and (b) the SOC corresponding to the specified OCVs at 0 °C, 20 °C, and 40 °C.

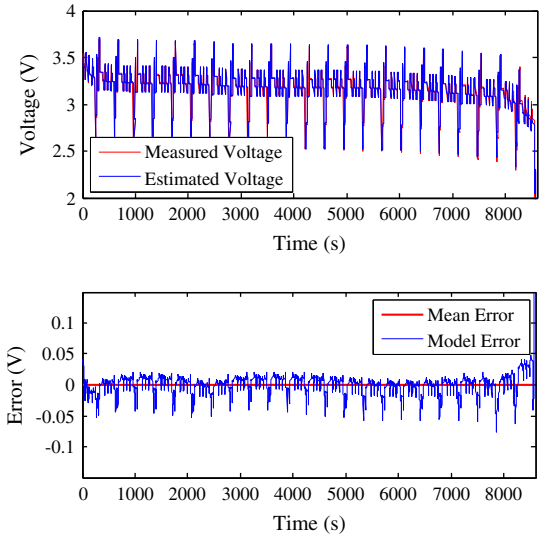

Fitted results of the developed model

Fig. 8. The measured and the estimated voltage response on the DST profile based on the proposed model at 20 °C.

Table 3
Fitted model parameter list and statistics list of model fitting.

T (°C)	R (Ω)	C	Mean absolute errors (V)	RMS modeling errors	Corrcoef (e_k, I_k)
0	0.2780	−0.0552	0.0153	0.0188	1.36e−13
10	0.2396	−0.0436	0.0112	0.0134	8.45e−14
20	0.2249	−0.0360	0.0087	0.0105	1.09e−13
25	0.2020	−0.0326	0.0080	0.0095	1.02e−13
30	0.1838	−0.0289	0.0073	0.0085	−7.62e−13
40	0.1565	−0.0237	0.0060	0.0071	2.85e−13
50	0.1816	−0.0201	0.0099	0.0131	3.15e−14

used for curve fitting while C(50 °C) was used to test the fitted performance of this exponential function. The 95% prediction bounds are shown in Fig. 9 based on C values and fitted curve. Apparently, C(50 °C) drops within the 95% prediction bounds. It can be seen that the function of $C(T)$ in Fig. 9 can be used to estimate C when the corresponding temperature test has not been run.

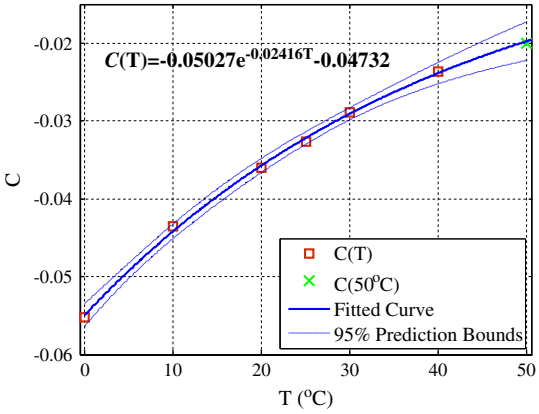

Fig. 9. Curve fitting for $C(T)$ and C(50 °C) for model validation.

4. Algorithm implementation for online estimation

The online SOC estimation has strong nonlinearity. This point can be seen from any battery model in which OCV has a nonlinear relationship with SOC. Additionally, the uncertainties due to the model inaccuracy, measurement noise, and operating conditions will cause a large variation in the estimation. The model-based nonlinear filtering approach has been developed to implement dynamic SOC estimation. The objective is to estimate the hidden system state, estimate the model parameters for system identification, or both. Thus, an error-feedback-based unscented Kalman filtering approach is proposed by shifting the system noise to improve the accuracy of the estimation.

4.1. Unscented Kalman filtering

The extended Kalman filtering (EKF) technique has become a popular technique for addressing the issue of state or parameter estimation for nonlinear systems. The rationale behind EKF is still the KF approach based on state space modeling. It aims to utilize the error between the current measurement and the model output to adjust the model state by virtue of a Kalman gain. Its principle and implementation can be found in [31]. Since KF is only available for linear systems, extended Kalman filtering (EKF) used a linearization process at each time step to approximate a nonlinear system through the first-order Taylor series expansion [31,32]. However, the first order approximation will probably lead to large errors in

Table 4
Summary of the UKF approach for SOC estimation.

- Initialize:
  - Measure ambient temperature, prepare $U_{OCV}(SOC, T)$ and R_0, C_0
  - Initial guess: S_0,
  - Covariance matrix: P_o
  - Process and measurement noise covariance: $\sum_{w_0}, \sum_V$
- Generate sigma points at time $k-1$, $(k \in [1, \ldots, \infty])$:

$$\boldsymbol{\chi}_{k-1} = \begin{bmatrix} S_{k-1} \\ R_{k-1} \end{bmatrix} = [\bar{\boldsymbol{\chi}}_{k-1}, \bar{\boldsymbol{\chi}}_{k-1} + \sqrt{(n+\lambda)\boldsymbol{P}_{k-1}}, \bar{\boldsymbol{\chi}}_{k-1} - \sqrt{(n+\lambda)\boldsymbol{P}_{k-1}}]$$

- Predict the prior state mean and covariance
  - Calculate sigma points through state function:

$$\boldsymbol{\chi}^i_{k|k-1} = \begin{bmatrix} S^i_{k|k-1} \\ R^i_{k|k-1} \end{bmatrix} = \begin{bmatrix} S^i_{k-1} - \frac{I_{k-1}\times\Delta t}{C_n} \\ R^i_{k-1} \end{bmatrix}, \quad i = 1, \ldots, 2n$$

  - Calculate the prior mean and covariance:

$$\hat{\boldsymbol{x}}^-_k = \sum_{i=0}^{2n} w^i_m \boldsymbol{\chi}^i_{k|k-1}, \quad \boldsymbol{P}^-_k = \sum_{i=0}^{2n} w^i_c \left[\boldsymbol{\chi}^i_{k|k-1} - \hat{\boldsymbol{x}}^-_k\right]\left[\boldsymbol{\chi}^i_{k|k-1} - \hat{\boldsymbol{x}}^-_k\right]^T + \sum_w$$

- Update using the measurement function
  - Calculate sigma points $\boldsymbol{y}_{k|k-1} = U_{OCV}(S_{k|k-1}, T) - I_k \times R(T)_{k|k-1} + C(T)$
  - Calculate the propagated mean: $\hat{\boldsymbol{y}}^-_k = \sum_{i=0}^{2n} w^i_m \boldsymbol{y}^i_{k|k-1}$
  - Calculate the covariance of the measurement:

$$\boldsymbol{P}_{y^-_k y^-_k} = \sum_{i=0}^{2n} w^i_c [\boldsymbol{y}^i_{k|k-1} - \hat{y}^-_k]^T + \sum_v$$

  - Calculate the cross-covariance and the state and measurement:

$$\boldsymbol{P}_{x^-_k y^-_k} = \sum_{i=0}^{2n} w^i_c [\boldsymbol{\chi}^i_{k|k-1} - \hat{x}^-_k][\boldsymbol{y}^i_{k|k-1} - \hat{y}^-_k]^T$$

- Compute filter gain and update and achieve the posterior SOC estimation
  - Compute the filter gain: $K_k = \boldsymbol{P}_{x^-_k y^-_k} \boldsymbol{P}^{-1}_{y^-_k y^-_k}$
  - Update the posterior state mean: $S^+_k = S^-_k + K_k(y_k - \hat{y}^-_k)$
  - Update the posterior covariance: $\boldsymbol{P}_k = \boldsymbol{P}^-_k + K_k \boldsymbol{P}_{\boldsymbol{y}_k, \boldsymbol{y}_k} K^T_k$

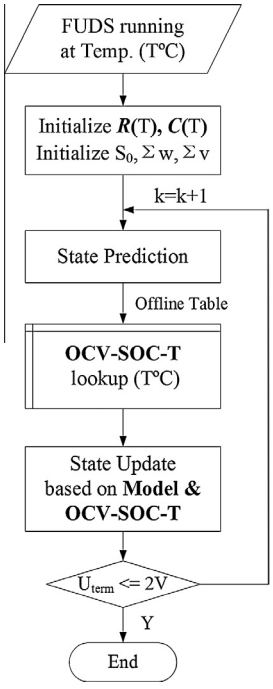

Fig. 10. The flow chart of battery SOC estimation by UKF based on OCV–SOC–*T* table.

the true posterior mean and covariance of the noise and could even result in divergence of the filter. Under this situation, unscented Kalman filtering (UKF) based on unscented transformation was suggested to avoid the weakness that comes from using Taylor series expansion.

The core idea of UKF is easier to approximate the state distribution that is represented by a minimal set of chosen sample points called sigma points, which can capture the mean and covariance of Gaussian random variable when propagated through a nonlinear system. The state-space model of a nonlinear system is represented as follows:

$$\begin{aligned} \boldsymbol{x}_k &= \mathbf{f}(\boldsymbol{x}_{k-1}, \boldsymbol{u}_{k-1}) + \boldsymbol{w}_{k-1} \\ \boldsymbol{y}_k &= \mathbf{h}(\boldsymbol{x}_k, \boldsymbol{u}_k) + \boldsymbol{v}_k \end{aligned} \tag{6}$$

where $\boldsymbol{x}_k$ is the system state vector and $\boldsymbol{y}_k$ is the measurement vector at time k. Correspondingly, $\mathbf{f}(\cdot)$ and $\mathbf{h}(\cdot)$ are the state function and the measurement function, respectively; $\boldsymbol{u}_k$ is the known input vector; $\mathbf{w}_k \sim \mathrm{N}(\mathbf{0}, \sum_{\mathbf{w}})$ is the Gaussian process noise; and $\mathbf{v}_k \sim \mathrm{N}(0, \sum_{\mathbf{V}})$ is the Gaussian measurement noise. Assume the state x has mean $\bar{x}$ and covariance P_x. Using the unscented transformation (UT), the state will be transformed as a matrix of $2n+1$ sigma vectors χ_i with corresponding weights w_i. These sigma points are shown in the following equation:

$$\begin{aligned} \boldsymbol{\chi}_{\boldsymbol{k}-1} &= [\bar{\boldsymbol{x}}^{(0)}_{\boldsymbol{k}-1}, \bar{\boldsymbol{x}}^{(1:n)}_{\boldsymbol{k}-1}, \bar{\boldsymbol{x}}^{(n+1:2n)}_{\boldsymbol{k}-1}] \\ &= [\bar{\boldsymbol{x}}_{\boldsymbol{k}-1}, \bar{\boldsymbol{x}}_{\boldsymbol{k}-1} + \sqrt{(n+\lambda)\boldsymbol{P}_{\boldsymbol{k}-1}}, \bar{\boldsymbol{x}}_{\boldsymbol{k}-1} - \sqrt{(n+\lambda)\boldsymbol{P}_{\boldsymbol{k}-1}}] \end{aligned} \tag{7}$$

where n is the dimension of the state and λ is a scaling parameter. These sigma points are propagated through a nonlinear function, re-estimated, and then they are used to capture the posterior mean and covariance to the 3rd Taylor expansion, as shown in Eqs. (9) and (10).

$$\mathbf{y}_\mathbf{i} = \mathbf{h}(\boldsymbol{\chi}_\mathbf{i}), \quad i = 0, \ldots, 2n \tag{8}$$

$$\bar{y} \approx \sum_{i=0}^{2n} w^{(i)}_m \mathbf{y}_\mathbf{i} \tag{9}$$

$$\boldsymbol{P}_y \approx \sum_{i=0}^{2n} w^{(i)}_c \{\boldsymbol{y}_i - \bar{\boldsymbol{y}}\}\{\boldsymbol{y}_i - \bar{\boldsymbol{y}}\}^T \tag{10}$$

where $w^{(i)}_m$ and $w^{(i)}_c$ are the weights of the corresponding sigma points that can be calculated in [33–35] for details.

4.2. SOC estimation based on proposed method

In our battery study, the state vector is $\boldsymbol{x} = [\mathrm{SOC}, R]^T$. The first state equation in Eq. (11) follows the coulomb counting method mentioned in Section 1. Peukert effect and capacity aging could be partially compensated when introducing the process noise $\omega_{1,k-1}$. A random walk is applied to the model parameter R regarding the cell-to-cell variation and operation uncertainties. Tuning the R will also be able to compensate for the variation of the C in our proposed model. The terminal voltage of the battery is the measured vector $\boldsymbol{y} = U_{\mathrm{term}}$, that is, the proposed battery model as shown in Eq. (5).

State function:

$$\begin{aligned} \mathrm{SOC}_k &= \mathrm{SOC}_{k-1} - I_{k-1} \times \Delta t / C_n + \omega_{1,k-1} \\ R_k &= R_{k-1} + \omega_{2,k-1} \end{aligned} \tag{11}$$

Measurement function:

$$U_{\mathrm{term},k} = U_{\mathrm{OCV}}(\mathrm{SOC}_k, T) - I_k \times R_k(T) + C(T) + v_k \tag{12}$$

where I_k is the current as the input (u_k in Eq. (6)) at time k; Δt is the sampling interval, which is 1 s according to the sampling rate; and C_n is the rated capacity. The rated capacity of the test samples is 1.1 Ah. And $\omega_{1,k}$, $\omega_{2,k}$ and v_k are zero-mean white stochastic processes with covariances $\sum_{\omega_1}$, $\sum_{\omega_2}$ and $\sum_v$, respectively. According to the proposed state-space model in Eqs. (11) and (12), the procedure of SOC estimation based on UKF is summarized in Table 4.

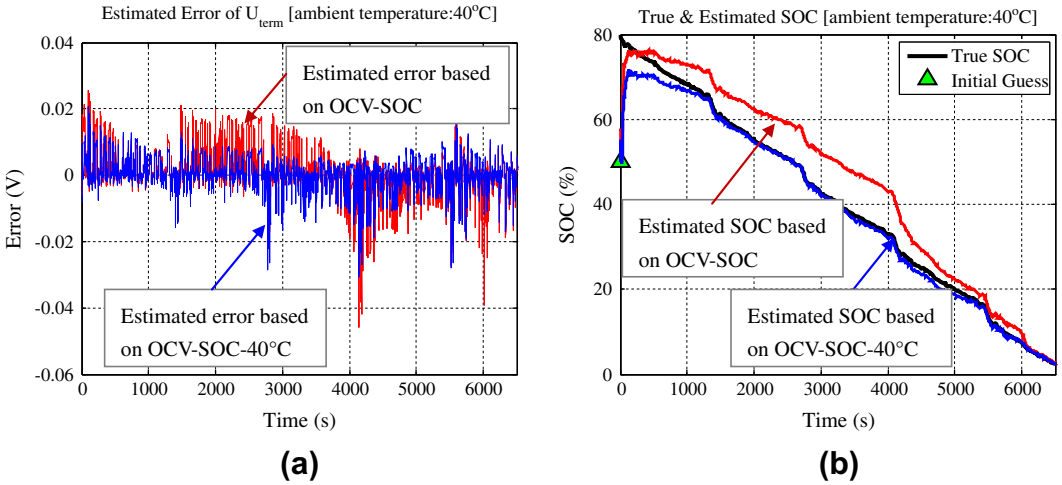

Fig. 11. The estimated comparison using two different OCV–SOC tables when FUDS was operated at 40 °C.

5. Experimental results for SOC estimation

Based on the temperature-based model, the developed method was validated using the FUDS test data, whose input and output are shown in Section 2.3. FUDS tests were run at different ambient temperatures to emulate the operation conditions. As analyzed in Section 3.2.1, we propose applying an OCV–SOC–*T* table instead of the conventional OCV–SOC lookup table, which was often established at room temperature, such as 25 °C. According to the measured ambient temperature (*T*), the corresponding OCV–SOC–*T* is employed as well as the updated model parameters, $R(T)$ and $C(T)$. A flow chart based on the OCV–SOC–*T* table is shown as Fig. 10. Model parameters will follow Table 3 according to the corresponding OCV–SOC table. A comparison will be made by using two lookup tables and their corresponding models. Initialized parameters, including the initial guess of S_0, measurement covariance, and process noise, were set the same for these two estimators.

Figs. 11 and 12 compare the results of the estimated SOC from two different lookup tables using UKF methods. Assuming that the original OCV–SOC table was tested at 25 °C, Fig. 11 shows the estimated results when a dynamic FUDS test was run at 40 °C. Fig. 11(a) shows the errors between the estimated terminal voltage (U_{term}) and the measured terminal voltage (U_{term}) based on OCV–SOC and OCV–SOC–40 °C, respectively. Fig. 11(b) shows the estimated SOC under these two OCV–SOC tables. Similarly, Fig. 12 presents similar estimated results when the FUDS profile was performed at 10 °C while referring to OCV–SOC and OCV–SOC–10 °C, respectively. For both of these two figures, the initial guess of SOC was set at 50%, while the true initial SOC was 80%.

As shown in Figs. 11 and 12(b), when the selected OCV–SOC–*T* table is consistent with the ambient temperature, the estimated value does capture the true SOC and converge fast. While using the original OCV–SOC, a large deviation from the true SOC will appear. Therefore, we recommend employing the OCV–SOC–*T* table according to a measured environmental temperature. Besides, the error of the estimated SOC at 10 °C is a bit larger than that at 40 °C. One reason is that the accuracy of the model at 10 °C is less than that at a higher temperature as shown in Table 3. The larger modeling error at low temperature is partially caused by the inaccuracy of the OCV–SOC at low temperature. The OCV hysteresis is a bit larger at low temperature. In addition, operation environment uncertainties would cause less improvement in battery SOC estimation at low temperature. The poor performance of the battery chemistry would present with a less releasable maximum capacity. It would make the battery model underperform, especially when the battery operates under high dynamic loading conditions.

For the untested temperature in OCV–SOC–*T*, i.e., 35 °C, the OCV–SOC–35 °C table can be constructed through linear interpolating between OCV–SOC–30 °C and OCV–SOC–40 °C. Although the errors do exist, the approximation can still reduce the effect of temperature on SOC estimation, which is necessary to save the testing time when it covers all the temperature range.

Tables 5 and 6 present a comparison of the estimation when the initial guess was at 30%, 50% and 70% SOC, while the true initial value covered its major working range from 25% to 85% SOC. The aim is to compare the effectiveness and robustness of the method in conjunction with the temperature-based model within the working range. The RMS estimated errors were calculated to assess and compare the estimated performance based on the original model and our developed model. Two points can be drawn from these tables. Firstly, under the conditions of different initial SOC values, the estimated results based on the temperature-based model will provide more accurate estimated results than the estimation without regard to temperature. The former have smaller RMS estimated errors, which are less than 4.7% at both 10 °C and 40 °C. Secondly, the estimated errors would be relatively larger when the true initial SOC is between 45% and 65%. The reason is that the OCV curve is flat in this phase, as shown in Fig. 3. Thus, a small deviation from the OCV inference will cause fluctuation of the estimated OCV. Estimating from this phase will take a longer time to converge to the true SOC.

Table 7 presents the estimated results at 0 °C as similar as Tables 5 and 6 show. Our method still showed an improvement on the SOC estimation. However, the maximum RMS estimated errors are up to 16.4%. The possible reason is that the battery performance deteriorates as temperature decreases due to the reducing rate of the internal chemical reaction. This is why preheating is necessary for a battery cranking at low temperature, as in EV. Its purpose is to make the battery operate up to a more efficient ambient temperature. Thus, our battery model performed well in most situations, except at a lower temperature condition, which may require a sophisticated model and a more accurate OCV–SOC curve considered. The investigation of the sophisticated model goes beyond the scope of this article.

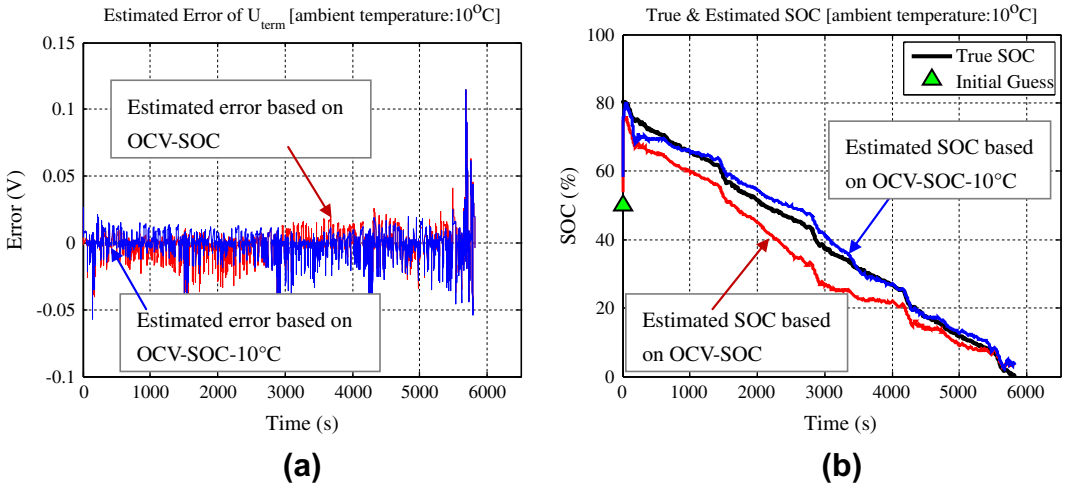

Fig. 12. The estimated comparison using two different OCV–SOC tables when FUDS was operated at 10 °C.

Table 5
RMSE (%) of SOC estimation when FUDS was run at 40 °C.

True Initial SOC (%)	OCV–SOC Initial guess of SOC (%)			OCV–SOC–40 °C Initial guess of SOC (%)		
	30	50	70	30	50	70
25	1.9266	1.9923	2.4692	1.1516	1.2221	1.9845
35	2.7525	2.5160	2.8922	1.1794	1.2200	1.6639
45	16.9565	16.4202	15.5435	2.7057	2.8986	2.8985
55	14.6350	14.5328	14.4129	4.5924	4.5315	4.6877
65	11.7265	11.5580	11.6536	4.5101	4.2905	4.4098
75	12.0255	11.9919	11.9558	1.5259	1.2580	0.9578
85	10.2871	10.2544	10.4074	2.8114	2.6363	2.6249

Table 6
RMSE (%) of SOC estimation when FUDS was run at 10 °C.

True Initial SOC (%)	OCV–SOC Initial Guess of SOC (%)			OCV–SOC–10 °C Initial Guess of SOC (%)		
	30	50	70	30	50	70
25	4.8945	4.3387	5.1118	2.3135	2.2842	2.6574
35	4.0763	4.0642	4.0150	1.7378	1.6058	1.9947
45	6.7356	6.7051	6.7183	3.9229	3.8942	3.9552
55	10.2816	10.3148	10.2542	3.1982	3.4937	3.3147
65	13.1890	13.1103	13.1261	4.0770	3.9304	3.8824
75	5.6472	5.4158	5.0041	2.6257	2.4144	2.2732
85	6.0865	6.1225	6.1734	2.2941	2.3679	2.1650

Table 7
RMSE (%) of SOC estimation when FUDS was run at 0 °C.

True Initial SOC (%)	OCV–SOC Initial guess of SOC (%)			OCV–SOC(0 °C) Initial guess of SOC (%)		
	30	50	70	30	50	70
25	4.9334	5.0495	6.6315	2.0551	2.2850	3.3146
35	11.3890	11.7336	11.6550	5.9619	6.1624	6.0038
45	10.8762	10.9386	10.8936	4.1374	4.1375	4.0302
55	16.7087	16.7250	16.7661	11.9187	12.2054	12.0170
65	18.5097	18.5317	18.5516	4.2343	4.1238	4.1266
75	24.6346	24.6161	24.5622	16.2830	16.3924	16.3719
85	12.3833	12.2986	12.3669	2.3437	2.2317	2.2520

6. Conclusions

Ambient temperature affects the relationship between open-circuit voltage (OCV) and SOC and, accordingly, influences model-based battery SOC estimation. In this paper, we developed a temperature-based battery model to address the temperature dependence of battery modeling. Firstly, our model is a simple and effective model that improves the accuracy of the estimated SOC

for lithium-ion batteries at different ambient temperatures. With few model parameters estimated, this model is easier and more computational efficient for on-board application. Secondly, an OCV–SOC–temperature table was applied in our model based on the OCV test with a temperature interval of 10 °C from 0 °C to 50 °C. The temperature dependence of the OCV–SOC table was concerned to improve the accuracy of the model. Finally, dynamic loading tests were run on the battery at different temperatures to assess the SOC estimation performance using the unscented Kalman filtering approach. A comparison was made between our battery model and the original model without regard to the temperature factor. The estimation covered the working range from 25% to 85% SOC. The results indicated that the estimation based on the developed battery model provided more accurate SOC values with smaller RMS estimated errors at different temperatures. The robustness of this method was verified under the conditions of three different initial SOC values. Thus, this approach could be successfully applied in BMSs for electric vehicles.

Two issues about the developed method are worthwhile to be mentioned here for an optimized online application. One is that the OCV–SOC–temperature table can be refined to save memory space in the online system by normalizing the temperature dependence of the OCV–SOC. The other is that the estimation based on our developed model provided a sufficiently accurate result with RMS estimated errors of less than 5% within the major working range. If there were a higher requirement on the estimated accuracy at temperature lower than even 0 °C, the SOC estimation based on a more sophisticated model would possibly make more sense.

Acknowledgements

The work presented in this paper was fully supported by a grant from the Research Grants Council of the Hong Kong Special Administrative Region, China (CityU8/CRF/09). The authors would like to thank the members of the Center for Advanced Life Cycle Engineering at the University of Maryland for their support of this work.

References

[1] Roscher MA, Sauer DU. Dynamic electric behavior and open-circuit-voltage modeling of $LiFePO_4$-based lithium ion secondary batteries. J Power Sources 2011;196:331–6.
[2] He H, Xiong R, Guo H. Online estimation of model parameters and state-of-charge of $LiFePO_4$ batteries in electric vehicles. Appl Energy 2012;89:413–20.
[3] Sun F, Hu X, Zou Y, Li S. Adaptive unscented Kalman filtering for state of charge estimation of a lithium-ion battery for electric vehicles. Energy 2011;36:3531–40.
[4] Wang D, Miao Q, Pecht M. Prognostics of lithium-ion batteries based on relevance vectors and a conditional three-parameter capacity degradation model. J Power Sources 2013;239:253–64.
[5] Xing Y, Ma EWM, Tsui KL, Pecht M. Battery management systems in electric and hybrid vehicles. Energies 2011;4:1840–57.
[6] He H, Zhang X, Xiong R, Xu Y, Guo H. Online model-based estimation of state-of-charge and open-circuit voltage of lithium-ion batteries in electric vehicles. Energy 2012.
[7] Junping W, Jingang G, Lei D. An adaptive Kalman filtering based state of charge combined estimator for electric vehicle battery pack. Energy Conv Manage 2009;50:3182–6.
[8] Johnson VH, Pesaran AA, Sack T. N.R.E. Laboratory, and S. America, temperature-dependent battery models for high-power lithium-ion batteries: National Renewable Energy Laboratory; 2001.
[9] Kim J, Lee S, Cho B. The state of charge estimation employing empirical parameters measurements for various temperatures. In: Power Electronics and Motion Control Conference, IPEMC'09, IEEE 6th International; 2009, p. 939–44.
[10] Plett GL. Extended Kalman filtering for battery management systems of LiPB-based HEV battery packs: Part 2. Modeling and identification. J Power Sources 2004;134:262–76.
[11] Lee S, Kim J, Lee J, Cho BH. State-of-charge and capacity estimation of lithium-ion battery using a new open-circuit voltage versus state-of-charge. J Power Sources 2008;185:1367–73.
[12] Cho S, Jeong H, Han C, Jin S, Lim JH, Oh J. State-of-charge estimation for lithium-ion batteries under various operating conditions using an equivalent circuit model. Computers Chem Eng 2012;41:1–9.
[13] Charkhgard M, Farrokhi M. State-of-charge estimation for lithium-ion batteries using neural networks and EKF. Indust Electron IEEE Trans 2010;57:4178–87.
[14] Ng KS, Moo C-S, Chen Y-P, Hsieh Y-C. Enhanced coulomb counting method for estimating state-of-charge and state-of-health of lithium-ion batteries. Appl Energy 2009;86:1506–11.
[15] Li IH, Wang WY, Su SF, Lee YS. A merged fuzzy neural network and its applications in battery state-of-charge estimation. Energy Conv IEEE Trans 2007;22:697–708.
[16] Bo C, Zhifeng B, Binggang C. State of charge estimation based on evolutionary neural network. Energy Conv Manage 2008;49:2788–94.
[17] Wang J, Chen Q, Cao B. Support vector machine based battery model for electric vehicles. Energy Conv Manage 2006;47:858–64.
[18] Plett GL. Sigma-point Kalman filtering for battery management systems of LiPB-based HEV Battery packs: Part 2. Simultaneous state and parameter estimation. J Power Sources 2006;161:1369–84.
[19] Hu X, Li S, Peng H. A comparative study of equivalent circuit models for Li-ion batteries. J Power Sources 2011;198:359–67.
[20] He H, Xiong R, Zhang X, Sun F, Fan J. State-of-charge estimation of lithium-ion battery using an adaptive extended Kalman filter based on an improved Thevenin model. Veh Technol IEEE Trans 2011. p. 1–1.
[21] Plett GL. Extended Kalman filtering for battery management systems of LiPB-based HEV battery packs: Part 1. Background. J Power Sources 2004;134:252–61.
[22] Plett GL. Extended Kalman filtering for battery management systems of LiPB-based HEV battery packs: Part 3. State and parameter estimation. J Power Sources 2004;134:277–92.
[23] Plett GL. Sigma-point Kalman filtering for battery management systems of LiPB-based HEV battery packs: Part 1. Introduction and state estimation. J Power Sources 2006;161:1356–68.
[24] Scrosati B, Garche J. Lithium batteries: status, prospects and future. J Power Sources 2010;195:2419–30.
[25] Kim J, Lee S, Cho B. The state of charge estimation employing empirical parameters measurements for various temperatures; 2009. p. 939–44.
[26] He W, Williard N, Osterman M, Pecht M. Prognostics of lithium-ion batteries based on Dempster–Shafer theory and the Bayesian Monte Carlo method. J Power Sources 2011;196:10314–21.
[27] Hunt G. USABC Electric Vehicle Battery Test Procedures Manual, ed: Rev; 1996.
[28] Dai H, Wei X, Sun Z, Wang J, Gu W. Online cell SOC estimation of Li-ion battery packs using a dual time-scale Kalman filtering for EV applications. Appl Energy 2012;95:227–37.
[29] Sun F, Xiong R, He H, Li W, Aussems JEE. Model-based dynamic multi-parameter method for peak power estimation of lithium–ion batteries. Appl Energy 2012;96:378–86.
[30] Waag W, Käbitz S, Sauer DU. Experimental investigation of the lithium-ion battery impedance characteristic at various conditions and aging states and its influence on the application. Appl Energy 2012;102:885–97.
[31] Bishop G, Welch G. An Introduction to the Kalman Filter, University of North Carolina at Chapel Hill, 2001 (Lesson Course).
[32] Arulampalam MS, Maskell S, Gordon N, Clapp T. A tutorial on particle filters for online nonlinear/non-Gaussian Bayesian tracking. Signal Process IEEE Trans 2002;50:174–88.
[33] Wan EA, Van Der Merwe R. The Unscented Kalman Filter, Kalman Filtering and, Neural Networks; 2001. p. 221–80.
[34] Wan EA, Van Der Merwe R. The unscented Kalman filter for nonlinear estimation. In: Adaptive Systems for Signal Processing, Communications, and Control Symposium. AS-SPCC. The IEEE 2000; 2000. p. 153–8.
[35] Miao Q, Xie L, Cui H, Liang W, Pecht M. Remaining useful life prediction of lithium-ion battery with unscented particle filter technique. Microelectron Reliab 2012;53:805–10.